2011

Evolution of stir zone microstructure during FSP of cast NiAl bronze

Menon, Sarath K.; England, Carolyn J.; McNelley, Terry R.

TMS (The Minerals, Metals & Materials Society)

http://hdl.handle.net/10945/56083

Friction Stir Welding and Processing VI
Edited by: Rajiv Mishra, Murray W. Mahoney, Yutaka Sato, Yuri Hovanski, and Ravi Verma
TMS (The Minerals, Metals & Materials Society), 2011

Evolution of Stir Zone Microstructure during FSP of Cast NiAl Bronze

Sarath K. Menon, Carolyn J England and Terry R. McNelley

Center for Materials Science and Engineering
Department of Mechanical and Aerospace Engineering
Naval Postgraduate School
Monterey, CA 93943-5146 USA

Keywords: NiAl Bronze; Friction Stir Processing; As-Cast; Stir Zone Microstructures

Abstract

The evolution of the stir zone microstructure during single-pass and multi-pass FSP of an as-cast NiAl bronze material was evaluated by optical and high-resolution scanning electron microscopy (SEM) methods, including orientation imaging microscopy (OIM). Deformation commences ahead of the tool as the local temperature exceeds the eutectoid temperature (≈800°C) while subsequent recrystallization in the primary α is accompanied by dissolution of κ_{IV} particles dispersed in this constituent. The recrystallized α grains remain equiaxed and appear annealed despite large displacements onward into the resulting stir zone (SZ). Characteristic shear texture components are retained in the thermomechanically affected zone (TMAZ) but the texture of the primary α becomes random after recrystallization and remains so into both single-pass and multi-pass SZs. Mechanisms to account for recrystallization and subsequent deformation are proposed.

Introduction

Multi-pass FSP can provide localized modification of microstructure and improvement in mechanical properties in near-surface regions of as-cast NiAl bronze materials [1]. FSP has been the subject of recent reviews [e.g, 2, 3]. Briefly, a non-consumable rotating tool that consists of a cylindrical shoulder region and a projecting, concentric pin of smaller diameter is forced against the surface of a deformable material. Initially, frictional heating softens the material so that the pin begins to penetrate the surface. Subsequently, the additional effect of sticking friction leads to plastic deformation under adiabatic conditions, and further heating and deformation in a column of material that forms around the pin. The pin continues to penetrate until the tool shoulder comes into contact with the material surface. The shoulder acts to constrain upward flow of deforming material and forge the resulting SZ while additional deformation is induced by action of the tool shoulder on the material surface. When the SZ has attained sufficient temperature the tool may be traversed in a pre-determined pattern over the surface to process a volume of material defined by the tool pin profile and processing pattern. In practice, the distance between adjacent traverses (i.e., the step over distance) must be kept small enough to insure overlap of successive SZs. FSP is an allied process of friction stir welding (FSW) [4]. The latter has been employed mainly in joining of wrought metals while FSP has been applied to both wrought and cast metals. FSW and FSP have been applied to alloys of Al and Mg as well as higher melting alloys of Cu, Fe and Ti [2,3].

The FSP thermomechanical cycle involves rapid transients and steep gradients in strain, strain rate and temperature within the resulting SZ [5]. Thus, when applied to a cast metal, FSP may convert the as-cast microstructure to a wrought condition in the absence of external shape change. The NiAl bronze alloy of interest in the present study is often used in large marine components such as propellers and, so, the as-cast microstructure evolves during very slow cooling at rates as low as $10^{-3}Cs^{-1}$. The severe deformation and much more rapid cooling during

FSP have a refining and homogenizing effect on the as-cast microstructure [5-8]. The resulting SZ material exhibits increased yield and ultimate strengths as well as greatly enhanced ductility, and such property improvement may enhance component service performance and reliability [1]. Nevertheless, the steep gradients in strain, strain rate and temperature also lead to gradients in microstructure and physical and mechanical properties that may lead, in turn, to strain localization and poor apparent properties during testing. Improved control and understanding of component properties and performance will require better understanding of the microstructures that develop in the complex deformation and temperature field of FSP. The evolution of SZ microstructure will be examined at locations in the vicinity of the tool pin extraction site in material subjected to a single pass and in a transverse section through the outermost pass in material subjected to multi-pass processing.

Experimental Procedures

The NiAl bronze material of this investigation has been described previously. Plates nominally 300 × 150 × 19mm^3 were machined from a large marine casting. Alloy composition data are provided in Table I. This material conforms to UNS95800.

Table I. Composition Data for the NiAl Bronze (UNS95800)

Element	Cu	Al	Ni	Fe	Mn	Si	Pb
Min-Max	(min)79.0	8.5-9.5	4.0-5.0	3.5-4.5	0.8-1.5	0.10(max)	0.03(max)
Nominal	81	9	5	4	1	-	-
Alloy	81.3	9.7	4.46	3.68	1.24	0.06	<0.005

One plate was subjected to a single-pass FSP run approximately 200mm in length using a Densimet®176 tool with a shoulder diameter of 28.6mm. The pin was 12.7mm long and in the shape of a truncated cone having a base diameter of 15mm and a tip diameter of 6.3mm. The pin also had a stepped spiral feature on its surface. This run involved a tool rotation rate of 1000rpm and a traversing rate of 50.8mm min^{-1} with the tool tilted 3° away from the traversing direction. Another plate was processed using a rectangular spiral pattern with a step over distance of 4.5mm such that each point in the resulting SZ experienced at least two passes by the tool. The same rpm, traversing rate and tool tilt were used for the multi-pass processing.

For optical microscopy, grinding and polishing were followed by etching in a two-step process involving, first, immersion for 1 – 2s in a solution of 40ml water – 40ml ammonium hydroxide – 2ml hydrogen peroxide (30pct.) and rinsing in water, and then followed by, second, immersion for 1 – 2s in a solution of 60ml water – 30ml phosphoric acid – 10ml hydrogen peroxide. Etched samples were examined using bright-field illumination in a Nikon Epiphot 200^{TM} inverted metallurgical microscope equipped with a CCD camera and computer system for image capture and analysis. Samples for SEM were electro-polished in a nitric acid – methanol solution containing 30pct. nitric acid and maintained at 0°C and using a voltage of 15V for 5 – 10s. All SEM examination was conducted using a Zeiss Neon 40^{TM} Field-Emission SEM (FE-SEM) operating at an accelerating voltage of 20kV in either secondary or backscatter imaging modes. OIM analysis was conducted using an EDAX-TSL system equipped with a Hikari^{TM} camera andcomputer system for image capture and re-construction.

Results and Disscussion

Fig. 1 is a montage of optical micrographs obtained on a plane perpendicular to the tool rotation axis and located at the mid-depth of the SZ at the extraction site of the tool for the single-pass traverse. The tool was moving in the direction toward the top of the page and the sense of tool rotation is indicated by the arrow. The advancing side (surface speed of the tool and traversing speed are additive) of the tool is to the right and the retreating side (surface speed of the tool and traversing speed subtract) is to the left in this montage. A pattern of deformation surrounding pin extraction site is apparent in the distortion of the microstructure constituents of this alloy.

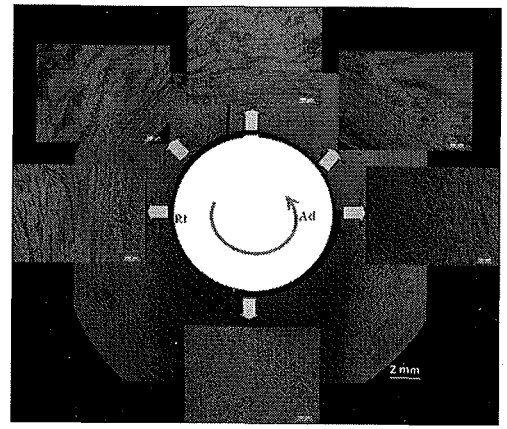

Figure 1. A montage of optical micrographs from the mid-depth of the SZ showing the deformation field around the tool pin. The tool was traversing toward the top of the page.

Details of the constitution of this alloy have been provided in previous publications [5-20]. Briefly, material conforming to the composition limits given in Table I solidifies at ≈1050°C as a bcc β phase. During equilibrium cooling, the primary α fcc terminal solid solution begins to form in the β with a Widmanstätten morphology at ≈1000°C. Globular κ_{ii} particles that are nominally Fe_3Al having a DO_3 structure begin to precipitate in the remaining β phase at ≈930°C while finer κ_{iv} particles that are also Fe_3Al commence precipitating in the α phase at ≈860°C. During cooling from ≈1000°C the β phase volume fraction decreases about linearly until the eutectoid decomposition reaction $\beta \rightarrow \alpha + \kappa_{iii}$ takes place over the temperature range from 800°C - 760°C and results in a eutectoid constituent having a lamellar morphology. The κ_{iii} phase is nominally NiAl having a B2 structure.

Heating during FSP leads to reversion of the eutectoid with the formation of β in locations experiencing temperatures above ≈800°C, and the phases in the resulting duplex α/β microstructure apparently deform compatibly under the action of the tool. The β transforms on cooling after passage of the tool but at rates much higher than during prior casting. The resulting β transformation products may include a refined lamellar eutectoid constituent or a bainitic or even martensitic product. All of the latter constituents tend to etch more darkly than the primary α. The relative volume fractions of primary α and β transformation products may be used to estimate local peak temperatures in the SZ and distortion of these constituents may used to estimate local strains in the TMAZ. Nevertheless, the mechanisms of refinement of the SZ microstructure and of deformation in the duplex microstructures of the TMAZ and SZ remain to be determined.

The as-cast microstructure from a location approximately 5mm ahead of the pin extraction site is shown in the OIM data of Fig. 2. In the image quality (IQ) map, Fig. 2a, the primary α contains dispersed κ_{iv} particles while the larger, globular κ_{ii} are dispersed in the eutectoid constituent and into the primary α, reflecting their formation over a large temperature range downward from 930°C. In this region, the grain-to-grain misorientation distribution, Fig. 2b, and the point-to-origin misorientation traverse in Fig. 2c (that corresponds to the traversing line in Fig. 2a) are consistent with the presence of high angle boundaries. The discrete pole figures in Fig. 2d suggest that the coarse grains of the primary α have random orientations.

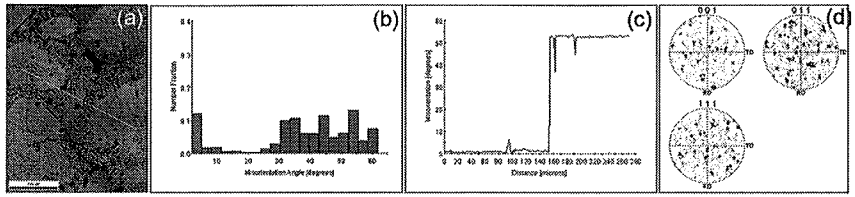

Figure 2. The as-cast microstructure is shown in the OIM data as an image quality (IQ) map in (a). The grain-to-grain misorientation distribution in (b) shows the predominance of high-angle boundaries and the point-to-origin misorientation distribution in (c) is consistent with the coarse-grained, as-cast microstructure. The discrete pole figures in (d) show that the grains have random lattice orientations.

The outer edge of the TMAZ is about 2mm ahead of the tool in Fig. 1 and OIM data in Fig. 3 show the characteristics of the onset of deformation at this location due to the action of the tool. The IQ map in Fig. 3a suggests the presence of a sub structure and the presence of low-angle (misorientation ≤5°) and moderately misoriented (5° < misorientation ≤15°) boundaries in the misorientation distribution in Fig. 3b is consistent with sub structure formation. A point-to-origin misorientation traverse in Fig. 3c (corresponding to the traversing line in Fig. 3a) indicates the buildup of long-range lattice curvature due to the development of the sub structure. The discrete pole figures in Fig. 3d show that this lattice curvature is related to a B-type shear texture component involving lattice rotation about a <011> axis that, in turn, is inclined to the tool axis in a plane perpendicular to the local surface of the tool.

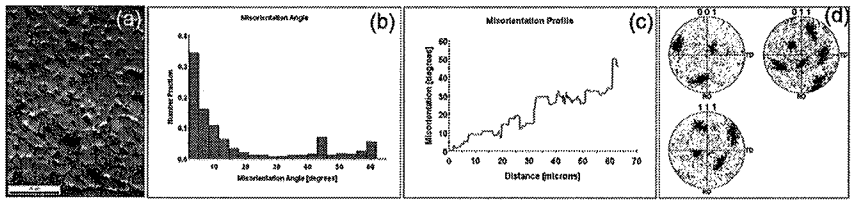

Figure 3. The microstructure at the outer edge of the TMAZ comprises mainly a sub structure within the primary α, as shown in the IQ map in (a). The grain-to-grain misorientation distribution in (b) shows the development of a large population of low-angle boundaries (misorientation ≤15°) while a point-to-origin misorientation distribution in (c) shows the presence of long-range lattice curvature. Such curvature is also reflected in the presence of a B-type shear texture component in the discrete pole figures in (d).

At locations closer to the tool and onward into the resulting SZ there is a distinct change in the nature of the microstructure. This is illustrated in Fig. 4 from a location in the SZ wherein material has been displaced a large distance around and toward the advancing side of the tool. At this location, the IQ map in Fig. 4a shows fine α grains in a banded structure and careful examination of this image reveals the presence of annealing twins. The grain-to-grain misorientation distribution in Fig. 4b indicates that the population of low-angle and moderately misoriented boundaries has decreased relative to that in the ourter TMAZ while the presence of twin boundaries is reflected in the peak at 60°. The point-to-origin misorientation distribution in Fig. 4c suggests that the long-range lattice curvature apparent at the outer edge of the TMAZ is no longer present. Instead, the microstructure consists of random boundaries and the discrete pole figures, Fig. 4c, indicate that lattice orientations are also random.

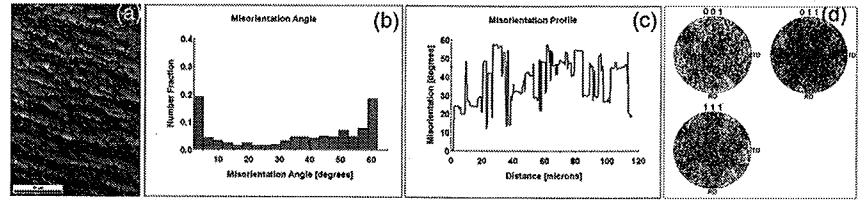

Figure 4. The IQ map in (a) shows the microstructure in the SZ nearby the tool pin. The recrystallized state of this microstructure is confirmed by the predominance of high-angle boundaries in the grain-to-grain misorientation distribution in (b) and in the point-to-origin misorientation distribution in (c). The discrete pole figures in (d) show a random texture that has developed in the SZ.

A transverse section through the outermost passes from multi-pass FSP of this same material are shown in the image of Fig. 5a; the advancing side of each pass is toward the right-hand side of this image. Upward flow of TMAZ material on the retreating side of the tool delineates successive passes. Details of the microstructure in a region that has experienced multiple passes are shown in Figs. 5b and c. These are secondary electron images from the FE-SEM examination of this material. The α phase grains appear equiaxed and are approximately 5μm in size, a value consistent with the grain size apparent in the SZ after a single pass (Fig. 4). Thus, the α grains apparently remain equiaxed despite very large displacements during deformation in multi-pass processing.

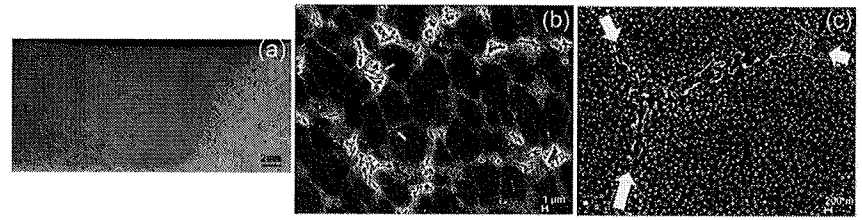

Figure 5. A transverse section including the outermost pass for multi-pass processing using a rectangular spiral pattern is shown in (a). High-resolution secondary electron images from FE-SEM examination of a region that has experienced two passes are included in (b) and (c). The arrows indicate the β transformation products formed upon cooling after FSP. These products were formed from the reaction $\alpha + \kappa_{iv} \rightarrow \beta$ within the primary α during heating above 860°C.

The high-resolution images in Figs. 5b and c also demonstrate a distinctive feature of the microstructure produced by multi-pass processing. In particular, the α grains do not exhibit well defined triple junctions. Instead, it appears that transformation products of β separate the α grains in a manner that suggests the spreading of β along α boundaries in association with the reaction peritectoid reaction $\alpha + \kappa_{iv} \rightarrow \beta$ as the κ_{iv} particles dissolved into the primary α constituent upon heating to local temperatures >860°C. This would likely occur in association with sub structure that had developed in the TMAZ during deformation and heating through the temperature interval 800°C - 860°C. The role of sub structure and κ_{iv} dissolution in the formation of the fine-grain SZ microstructure is summarized in the schematics of Fig. 6. Thus, deformation in the primary α leads to sub structure formation during heating from≈800° to ≈860°C as illustrated in Fig. 6a. The κ_{iv} dissolves beginning at 860°C and diffusion of the Fe component takes place

along the sub structure boundaries, as indicated in Fig. 6b. Spreading along the α/α boundaries in the sub structure would reflect the condition $\gamma_{\alpha\alpha} \leq \sqrt{3}\ \gamma_{\alpha\beta}$, where γ is the interfacial energy.

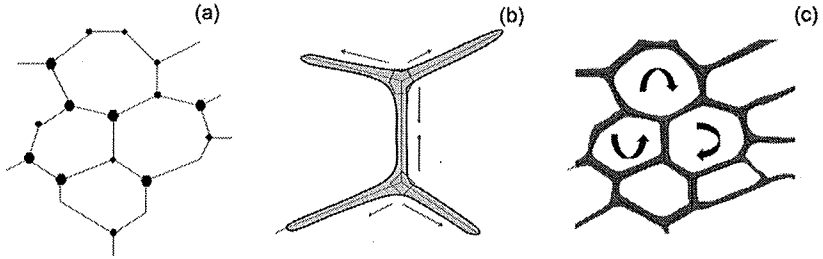

Figure 6. A schematic representation of a sub structure (the dotted lines) stabilized by the κ_{iv} particles in the primary α is shown in (a). The dissolution of the κ_{iv} and spreading of the resulting β along the α/α boundaries is depicted in (b). The presence of a continuous β phase in a very fine-grained duplex α/β microstructure may enable phase boundary sliding to occur during the deformation near peak temperature in FSP as illustrated in (c). This may account for the random textures observed in SZ microstructures.

The development of random grain orientations in the interior of the TMAZ and onward into the SZ would reflect random grain rotations in the resulting α/β duplex microstructure, as suggested in Fig. 6c. In turn, this would be feasible only if the α/β interfaces were able to sustain phase-boundary sliding during FSP. While the deformation involves high strain rates the peak deformation temperatures apparently approach $0.95T_{Melt}$ with only a very brief dwell at such a TMAZ temperature. This would suppress grain growth and facilitate dominance of phase boundary sliding.

Conclusions

The following conclusions may be reached from this investigation.

- The coarse-grained as-cast microstructure begins to deform as the local temperature exceeds the eutectoid temperature and the eutectoid constituent reverts to form β. Sub structure, stabilized by dispersed κ_{iv} particles, develops in the primary α in the temperature interval 800°C - 860°C.
- The κ_{iv} dissolves along sub structure boundaries as the local temperature exceeds 860°C resulting in the formation of β in between new grains in the primary α. The grains in the primary α are typically 5μm in size.
- Phase boundary sliding in the duplex α/β structure can account for random grain orientations in the α grains within single-pass and multi-pass SZs.

Acknowledgement

Financial support for this work was provided by the Office of Naval Research under contract number N0001409WR20201 with Dr William Mullins as Program Officer.

References

1. T R McNelley, K Oh-Ishi and A P Zhilyaev: Chapter 8 in *Friction Stir Welding and Processing* (R.S. Mishra and M.W. Mahoney, eds.), ASM International, Materials Park, OH, 2007, pp. 155 – 174
2. R S Mishra and Z.Y. Ma: *Mater. Sci. Eng. R*, 2005, vol. 50, pp. 1 – 78
3. *Friction Stir Welding and Processing* (R.S. Mishra and M.W. Mahoney, eds.), ASM International, Materials Park, OH, 2007
4. W M Thomas, E D Nicholas, J C Needham, M G Murch, P Templesmith and C J Dawes: G. B. Patent Application No. 9125978.8, Dec. 1991; U. S. Patent No. 5460317, Oct. 1991
5. S Swaminathan, K. Oh-Ishi, A.P. Zhilyaev, C.B. Fuller, B. London, M.W. Mahoney and T.R. McNelley: *Metall. Mater. Trans. A*, 2010, vol. 41A, pp. 631 – 40
6. K. Oh-ishi and T. R. McNelley: *Metall. Mater. Trans. A*, 2004, vol.35A, pp 2951-61
7. K. Oh-ishi and T. R. McNelley: *Metall. Mater. Trans. A*, 2005, vol. 36A, pp. 1575-85.
8. K. Oh-Ishi, A. P. Zhilyaev and T. R. McNelley: *Metall. Mater. Trans. A*, 2006, vol. 37A, pp. 2239-51
9. P. Weill-Couly and D. Arnaud: *Fonderie*, 1973, no. 322, p. 123-35
10. E.A. Culpan and G. Rose: *J. Mater. Sci.*, 1978, vol. 13, p. 1647-57
11. E.A. Culpan and G. Rose: British Corrosion J, 1979, vol. 14, p. 160-166
12. D.M. Lloyd, G.W. Lorimer and N. Ridley: *Metals Technology*, 1980, vol. 7, p. 114-19
13. P. Brezina: *Int. Met. Rev.*, 1982, vol. 27, p. 77-120
14. F. Hasan, G.W. Lorimer and N. Ridley: Proc. Intl. Conf. On Solid to Solid Phase Transformations, TMS, Warrendale, PA, 1982, p. 745-49
15. F. Hasan, A. Jahanafrooz, G.W. Lorimer and N. Ridley: *Metall. Trans. A*, 1982, vol. 13A, p. 1337-45
16. F. Hasan, G.W. Lorimer and N. Ridley: *Journal de Physique*, 1982, vol. 43, p. C4 653-58
17. A. Jahanafrooz, F. Hasan, G.W. Lorimer and N. Ridley: *Metall. Trans. A*, 1983, vol. 14A, p. 1951-56
18. F. Hasan, G.W. Lorimer and N. Ridley: *Metal Sci.*, 1983, vol. 17, p. 289-95
19. F. Hasan, J. Iqbal and N. Ridley: *Mater. Sci. Tech.*, 1985, vol. 1, p. 312-15
20. G.W. Lorimer, F. Hasan, J. Iqbal and N. Ridley: *British Corrosion J.*, 1986, vol. 21, p. 244-48